ACTA TECHNICA CORVINIENSIS – Bulletin of Engineering | e–ISSN: 2067 – 3809
Tome XVIII [2025] | Fascicule 1 [January – March]

[1.]Samuel Chiedu OKONKWO, [2.]Victoria Dumebi OBASA, [1.]Kolawole Dayo ALONGE,
[1.]Isaac Efe ODUARAN, [1, 3.]Samson Oluropo ADEOSUN

THE MECHANICAL, THERMAL, AND ELECTRICAL PROPERTIES OF AA2011 ALUMINUM/ KAOLIN/ METAKAOLIN COMPOSITES FOR TRANSPORT APPLICATIONS

[1.] Department of Metallurgical and Materials Engineering, University of Lagos, Lagos 101017, NIGERIA
[2.] Department of Industrial and Systems Engineering, Lagos State University, Lagos 102101, NIGERIA
[3.] Industrial Engineering Department, Durban University of Technology, Durban, SOUTH AFRICA

Abstract: The growing need for lightweight and durable materials in transportation requires the development of metal matrix composites (MMCs) with enhanced mechanical, thermal, and electrical properties. This research analyzes the effects of different weight percentages (2–10 wt.%) of kaolin and metakaolin as reinforcements in the AA2011 aluminum matrix. The composites were produced using stir casting, homogenized through heat treatment, and evaluated for tensile strength, thermal stability, crystal structure, microstructure, and electrical conductivity. The results showed a reduction in ultimate tensile strength (UTS) with both reinforcements, however, adding 4 wt.% metakaolin improved the ductility. The microstructural analysis revealed that higher filler contents alter uniform phase dispersion, causing clustering and microporosity. Thermal stability was notably enhanced, especially with 10 wt.% kaolin. The electrical conductivity of the composites displayed an inverse correlation with filler content specifically, at 4 wt.% metakaolin and 10 wt.% kaolin at low currents. These discoveries offer valuable insights into the potential use of kaolin and metakaolin–reinforced AA2011 in automobile components that demand strength, thermal stability, and electrical conductivity.
Keywords: composites, reinforcements, stir casting, kaolin and metakaolin

INTRODUCTION

The transportation sector is undergoing a transformative phase driven by the need for higher energy efficiency, reduced emissions, and more sustainable materials. Aluminum alloys, particularly AA2011, have garnered significant attention due to their excellent machinability, high corrosion resistance, and exceptional strength–to–weight ratio, making them ideal for transport applications like automotive and aerospace components [1,2]. However, a growing demand remains for materials that offer improved mechanical and thermal performance without compromising weight [3]. In this regard, metal matrix composites (MMCs) provide an ideal solution by incorporating ceramic reinforcements into the base metal to enhance its properties [4].

Among potential ceramic reinforcements, kaolin and metakaolin are attractive due to their availability, cost–effectiveness, and favorable physical properties [5]. Kaolin, a naturally occurring aluminosilicate clay, can be thermally treated to form a more reactive phase of metakaolin [6]. The calcination process, typically conducted at around 800°C, removes water from the kaolin structure, resulting in a disordered, amorphous material with improved mechanical and thermal properties [7, 8]. Adding kaolin or metakaolin into aluminum alloys can significantly alter the composite's microstructure and performance [9].

While adding ceramic reinforcements typically improves wear resistance and hardness, it can negatively impact the composite's ductility and tensile strength if not properly controlled [10]. For example, increasing the filler content beyond an optimal point often leads to particle agglomeration, resulting in stress concentration sites within the matrix. This can lead to premature failure during mechanical loading due to crack initiation at these points. Additionally, the size and distribution of the reinforcements play a critical role in defining the composite's behavior under load, with fine, well–dispersed particles showing better mechanical performance when compared to larger, clustered ones [11, 12].

The stir casting technique, used in this study to fabricate the composites, is a well–established method for producing MMCs. It is widely preferred for its cost–effectiveness and

scalability, making it suitable for industrial applications. However, one of the primary challenges in stir casting is ensuring a uniform distribution of the reinforcement particles within the matrix [3, 4]. The effectiveness of particle dispersion significantly influences the mechanical properties of the final composite. Poor wetting between the ceramic particles and the metal matrix, combined with potential agglomeration, can lead to defects like porosity and phase segregation. Addressing these challenges requires precise control over the processing conditions, including stirring time, speed, and temperature, to achieve a homogenous composite structure [13].

Thermal stability is another important consideration for MMCs, especially for applications in the transportation industry where components are often exposed to high temperatures. Kaolin and metakaolin addition is expected to enhance the thermal stability of AA2011 by forming thermally stable phases that could resist degradation at elevated temperatures [14]. Thermogravimetric analysis (TGA) provides valuable insights into the thermal performance of these composites, with previous studies showing that composites with ceramic reinforcements exhibit higher decomposition temperatures and slower weight loss compared to unreinforced aluminum alloys [15]. This enhancement in thermal properties is particularly beneficial for high–temperature applications such as engine components, where material degradation over time can significantly affect performance and safety [16].

In addition to mechanical and thermal properties, electrical conductivity is a key factor for materials used in transportation, particularly in the context of electric vehicles and power transmission systems. Adding insulating ceramic fillers such as kaolin and metakaolin into the aluminum matrix could reduce electrical conductivity [17]. However, the extent of this reduction depends on the filler content and distribution. With lower filler volume, the impact on conductivity may be minimal, allowing for adequate electrical properties while benefiting from mechanical improvements. Optimizing the balance between mechanical strength and electrical conductivity is critical for applications where both properties are important, as in structural components that serve as conductors.

This study examines the effects of adding kaolin and metakaolin (2, 4, 6, 8, and 10 wt.%) on the mechanical, thermal, and electrical properties of AA2011 aluminum alloy. The composites were characterized through tensile testing to determine their mechanical behaviours, X–ray diffraction (XRD) and scanning electron microscopy (SEM) for crystal structure and microstructural analysis respectively, thermogravimetric analysis (TGA) to assess thermal stability, and electrical conductivity tests to evaluate their performance under varying electrical loads. Recent studies on aluminum–based MMCs have focused on understanding the effects of ceramic particle reinforcements on their mechanical properties, thermal stability, and electrical performance.

EXPERIMENTAL PROCEDURE

Materials

This research was done at the University of Lagos Metallurgical Engineering laboratory. The base alloy used for this work is aluminium alloy (AA2011). Table 1 shows the compositional analysis. The reinforcements used in the investigation are kaolin and metakaolin. The kaolin samples were obtained from the Civil and Environmental Engineering Department University of Lagos, Nigeria. The metakaolin used was obtained from the calcination of kaolin powder. Tables 2 and 3 show the compositional analysis of both powders.

Methods

The kaolin filler was heated to 200°C in a Gallenkomp SXL–1008 model muffle furnace to keep it dry. To obtain the metakaolin, kaolin powder was heated in the muffle furnace to 800°C for 2 hours. Morgan crucible furnace was employed to heat the base alloy to 720°C. The slag was scooped off the surface of the molten base metal before the preheated kaolin was poured into it and stirred thoroughly for 2 minutes. The mould pattern was pre–heated before the mixture was poured to produce the samples. Once solidification had been completed, the casts were removed from the pattern and allowed to cool to room temperature. This process was repeated until all 15 samples with kaolin reinforcements were produced. The same thing was done to produce composite samples with metakaolin reinforcement.

Homogenization

The casting samples were homogenized by heat–treating them at 480°C for 8 hours in a Gallenkomp SXL–1008 model muffle furnace to

relieve them of stress acquired during the casting process.

CHARACTERIZATIONS OF ALUMINUM COMPOSITES

Tensile Test

The tensile test was carried out on a Hukoto testing machine. The samples were machined as per ASTM E8M standards. The gauge length and the diameter of the specimen were 25 mm and 5 mm respectively. A test speed of 100 mm/min was adopted. Each experiment was carried out thrice, and average taken.

Chemical Composition

An Olympus Metallurgical Microscope was used to carry out the optical microscopy of the distribution of the reinforcements in the composite. To view the samples, each of them was ground before polishing and etching. Emery papers of grades 60,123, 220, 320, 400, 600, 800, and 1,200 were used to ground the surfaces. They were etched in sodium hydroxide (NaOH) in distilled water at 70 °C for about 10 seconds. Further characterizations such as XRD were done to examine the phases present in the samples, SEM–EDS for greater depth of microstructural view with elemental analysis, TGA to analyze their thermal stability, and electrical test to compare their electrical stability.

Table 1. Chemical composition of AA2011

Constituent	Composition %
Al	95.590
Si	0.430
Fe	0.334
Cu	0.341
Mn	0.110
Mg	0.055
Zn	0.084
Cr	0.057
Ni	0.197
Ti	0.031
Zr	0.096
V	0.088
Ca	0.001

Table 2. Elemental Composition of Metakaolin at 800°C for 2 hours.

Element no	Symbol	Name	Atomic no	Weight %
8	O	Oxygen	64.45	59.88
6	C	Carbon	10.23	7.14
14	Si	Silicon	7.01	11.43
13	Al	Aluminium	8.85	13.86

Table 3. Elemental Composition of Kaolin

Element no	Symbol	Name	Atomic no	Weight %
8	O	Oxygen	64.45	59.88
6	C	Carbon	10.23	7.14
14	Si	Silicon	7.01	11.43
7	N	Nitrogen	9.46	7.7
13	Al	Aluminium	8.85	13.86

RESULTS AND DISCUSSION

Microstructural Evaluation

Figure 1 is the X–ray diffractogram (XRD) of AA2011 without filler, with 8 wt.% kaolin, and 4 wt. % metakaolin.

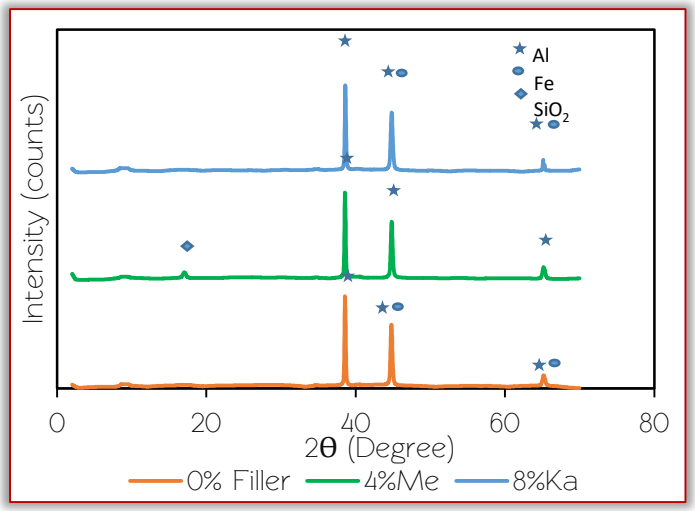

Figure 1. XRD of AA2011 composites with fillers.

The analysis revealed the presence of multiple phases with a scan range from 2⁰ to 70⁰ (2θ). Aluminium, the dominant phase showed the highest peak in all three samples. The most intense peak was at 44.76° while the lowest intense peak was at 17.02°. Peaks of other secondary phases present are aluminum–iron (Al–Fe) and silicon oxide (SiO_2). Aluminium–iron was present in AA2011 without filler and AA2011 + 8 wt. % kaolin.

Figure 2(a) presents SEM/EDS micrograph of control AA2011. Dark grey eutectic structures that are well distributed within the light grey a–aluminium matrix could be seen. The eutectic microstructure typically appears as a lamella of $CuAl_2$ particles within the aluminium matrix, contributing to increased strength and hardness [18].

Further analysis with image J software revealed a consistent structure without voids or agglomeration as shown in Figure 2(a). Figure 2 (d) captured regions with white floating particles indicative of the presence of traces of heavy insoluble second–phase particles or inclusion with distinct responses to etching compared to the surrounding matrix [19]. The rounded–shaped insoluble particles replicated throughout the SEM micrograph of kaolin in Figures 3d, 4d, and 5d can be attributed to alloying elements like copper, iron, and silicon contained in AA2011. These elements can form intermetallic compounds (e.g., Al_2Cu, Al_3Fe, or AlFeSi), which may appear as insoluble particles under a microscope.

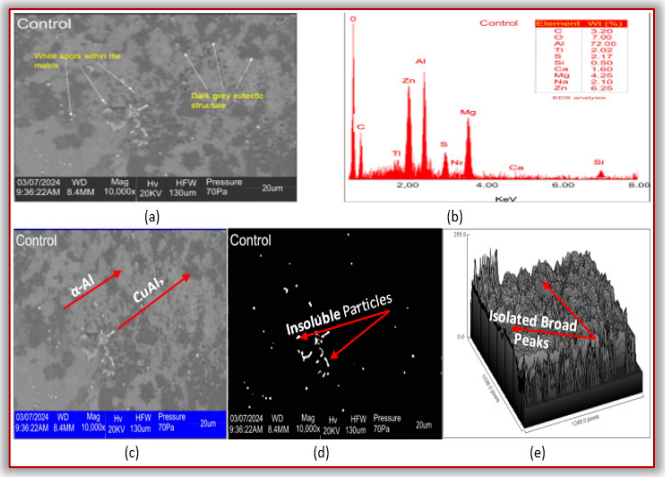

Figure 2. (a) SEM micrograph of control AA2011, (b) EDS, (c) Surface Morphology, (d) Distribution of insoluble particles, (e) 3D surface intensity

The different peaks in both kaolin and metakaolin reinforced composite show the elemental composition in descending order and ascending order as seen throughout the EDS in Figures 2b, 3b, 4c, 5b, 6b, 7b and 8b.

The absence of iron in the EDS analysis of the control sample could be because it is localized to a particular section of the sample not specifically analyzed by EDS as it is a surface–sensitive operation. It could also be that they are in forms or quantities below the detection limit of the EDS or due to distribution differences. This highlights the complementary nature of XRD in that it can detect crystalline phases that EDS might miss due to sensitivity limits.

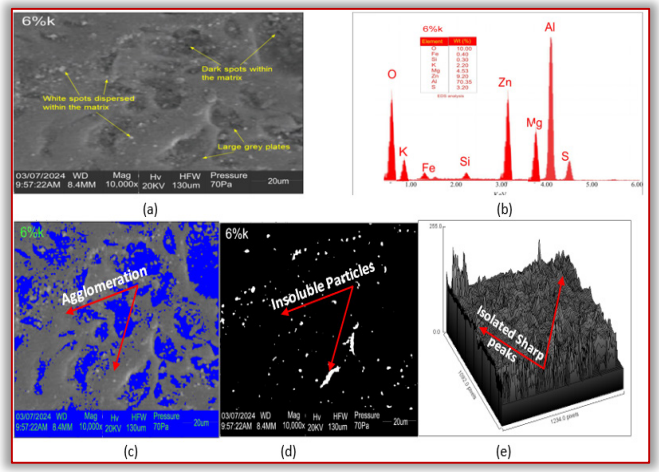

Figure 3. (a) SEM micrograph of AA2011 + 6 wt. % kaolin, (b) EDS, (c) Surface Morphology, (d) Distribution of insoluble particles, (e) 3D surface intensity

Figure 3 shows the SEM/EDS micrograph of AA2011 + 6 wt.% kaolin. The large grey plates represent regions of agglomeration as revealed by Figure 3c. The dark spots, which are sparsely dispersed within the matrix could be the kaolin reinforcement or silicon oxide phase. Here the floating white particle now consists of both rounded and irregular shapes. This could be because of aluminum oxide (Al_2O_3) inclusions which are potential defect sites [20].

AA2011 + 8 wt. % kaolin in Figure 4 presents a more heterogeneous kaolin reinforcement within the matrix. The sharp uniform intensity of Figure 4e confirms an overlapping scaly morphology which is evident in a complex microstructure resulting from increased particle–matrix of a network of Al–Fe and silicon oxide within the matrix [21].

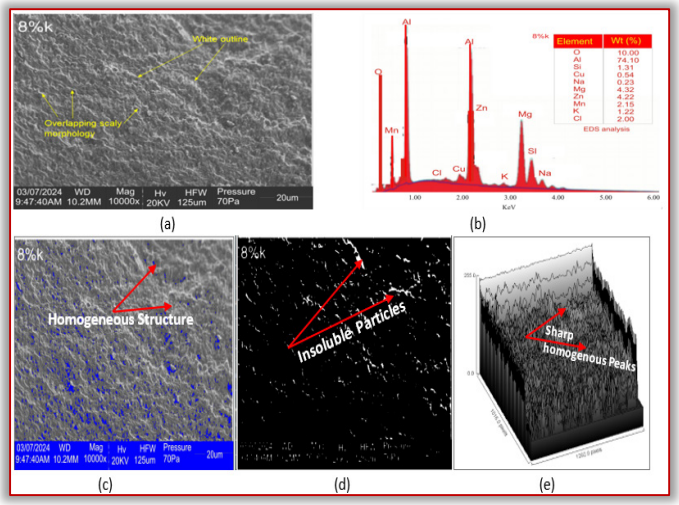

Figure 4. (a) SEMEDS micrograph of AA2011 + 8 wt. % kaolin(b) EDS, (c) Surface Morphology, (d) Distribution of insoluble particles, (e) 3D surface intensity

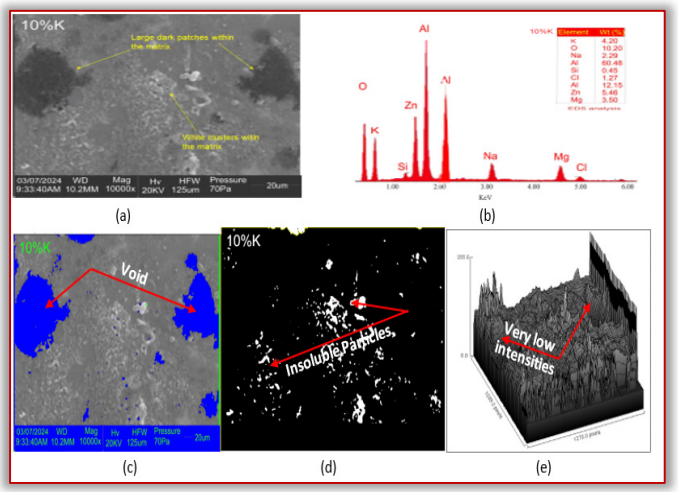

Figure 5. (a) SEM micrograph of AA2011 + 10 wt. % kaolin, (b) EDS, (c) Surface Morphology, (d) Distribution of insoluble particles, (e) 3D surface intensity

Also, Figure 5 shows the SEM/EDS micrograph of AA2011 + 10 wt. % kaolin. There is an increased segregation within the matrix. The larger dark patches seen could be aggregates of silicon oxide or kaolin. This excessive agglomeration could give rise to porosity within the microstructure. Also, an increased clustering of the white particles is observed within the structure. This general increase in phase segregation could lead to potential points of cracks or porosity around the kaolin particles

indicated as region on very low intensities in Figure 5e.

The SEM/EDS of AA2011 + 2 wt. % metakaolin exhibited a high degree of agglomeration as shown in Figure 6. Its rough morphology and micropores are indicated by dispersed intensities shown in Figure 6e These features negatively affect the mechanical properties of this composite such as the tensile strength and ductility. The elemental composition from the EDS analysis in descending order of weight percent are Al, O, Zn, Mg, C, Cu, Na, Cl, Ca, and Si. Aluminium having the highest weight percent in the composite confirms it as the primary phase in the XRD analysis. The presence of silicon and oxygen confirms the silicon oxide phase present in the XRD analysis. Other elements present contribute to forming the solid solution of the alloy.

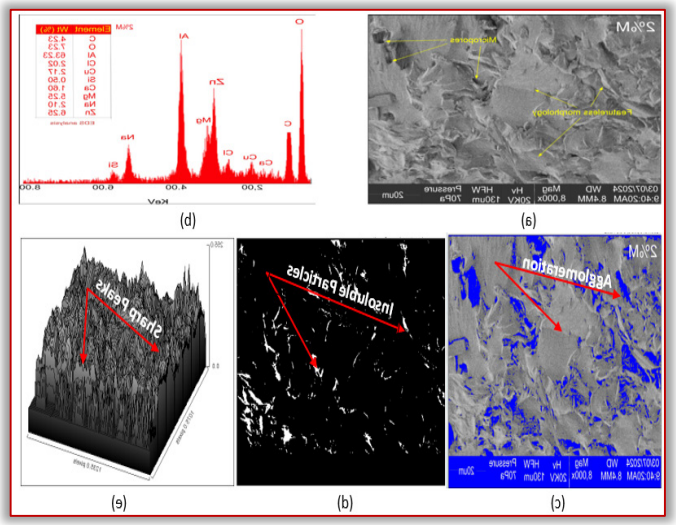

Figure 6. (a) SEM micrograph of AA2011 + 2 wt. % metakaolin, (b) EDS, (c) Surface Morphology, (d) Distribution of insoluble particles, (e) 3D surface intensity

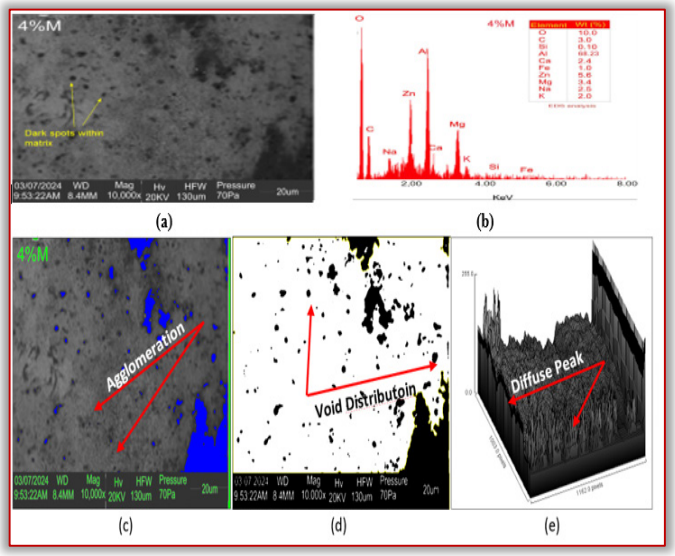

Figure 7. (a) SEM micrograph of AA2011 + 4 wt. % metakaolin, (b) EDS, (c) Surface Morphology, (d) Pore Distribution, (e) 3D surface intensity

Figure 7 presents the SEM/EDS of AA2011 + 4 wt. % metakaolin. It shows a better uniform structure than AA2011 + 2wt. % metakaolin with no observable floating insoluble particles but containing dark spots dispersed within the matrix [22]. Further software analysis showcased these dark spots as micropores, regions which are susceptible to stress concentrations, thus, lowering the tensile strength [23]. The elemental composition from the EDS shows presence of silicon and oxygen thereby confirming the silicon oxide phase present in the XRD analysis.

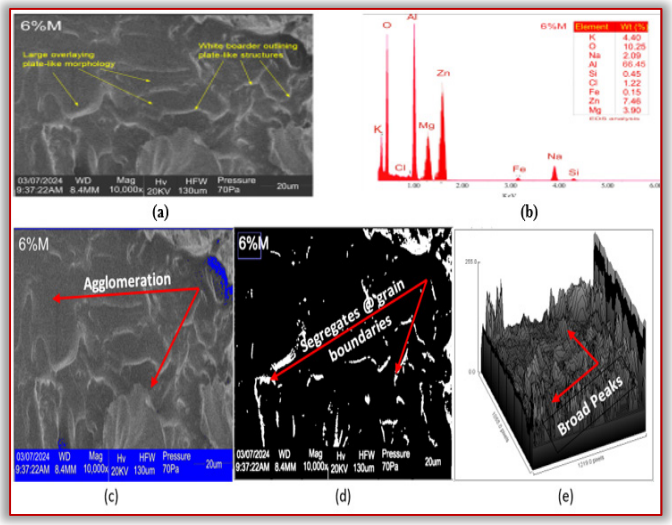

Figure 8. (a) SEM micrograph of AA2011 + 6 wt. % metakaolin, (b) EDS, (c) Surface Morphology, (d) Distribution of insoluble particles, (e) 3D intensity

The SEM/EDS of AA2011 + 6 wt. % metakaolin in Figure 8 exhibited a nonuniform surface morphology (agglomeration) and diffuse intensity as revealed in subfigures of c and e. It has a large overlaying plate–like morphology with a whitish needle–like outline around the grain boundaries. This shape morphology suggests the presence of $CuAl_2$ intermetallic phase which could significantly enhance strength and hardness of the structure. [24].

Metallographic Evaluation

Figure 9(a) shows the micrograph of control AA2011. It has an equiaxed microstructure with an even distribution of particles within the matrix and along the grain boundaries.

In Figure 9(b), AA2011 + 2 wt. % kaolin has a higher concentration of kaolin particles along the grain boundaries than within the matrix. Minimal clusters can also be seen within the composite.

Figure 9(c) shows the micrograph of AA2011 + 4 wt. % kaolin. There is a gradual increase in concentration and even dispersion of reinforcement in this composite at the grain boundaries and within the matrix.

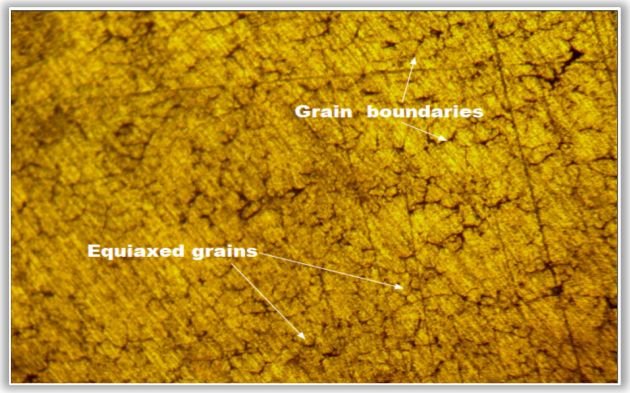

Figure 9(a). AA2011 + 0 wt. % filler

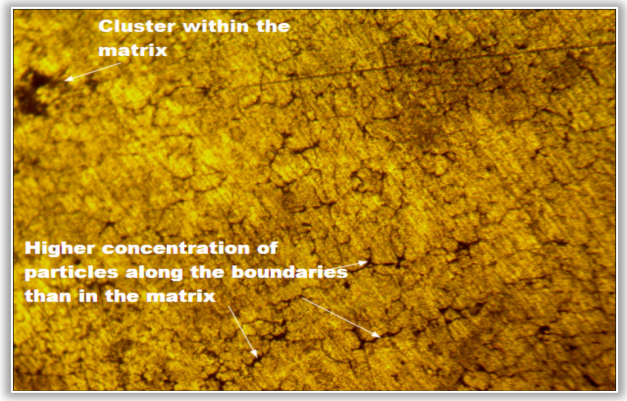

Figure 9(b). AA2011 + 2 wt. % kaolin

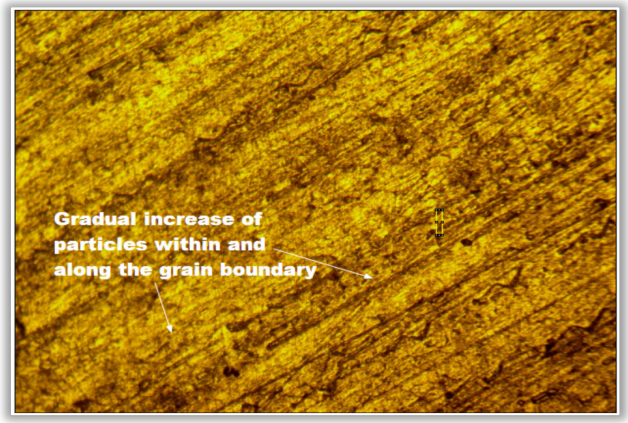

Figure 9(c). AA2011 + 4 wt. % kaolin

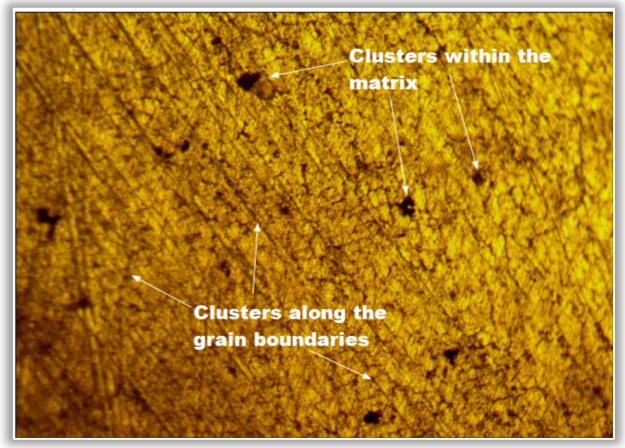

Figure 9(d). AA2011 + 6 wt. % kaolin

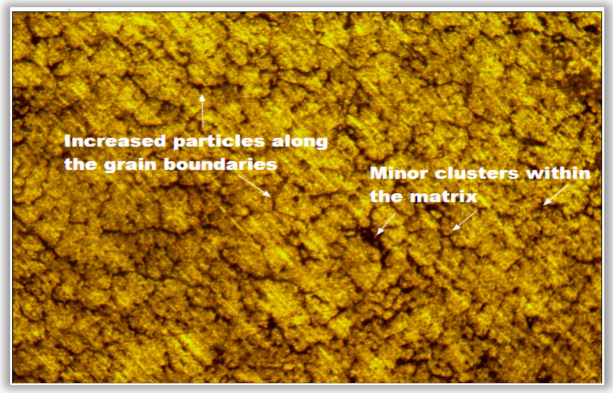

Figure 9(e). AA2011 + 8 wt. % kaolin

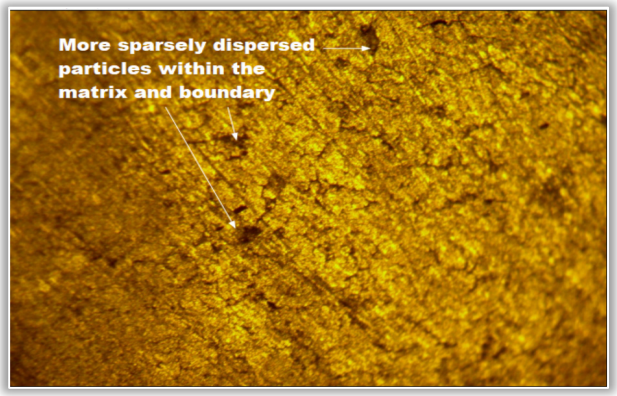

Figure 9(f). AA2011 + 10 wt. % kaolin

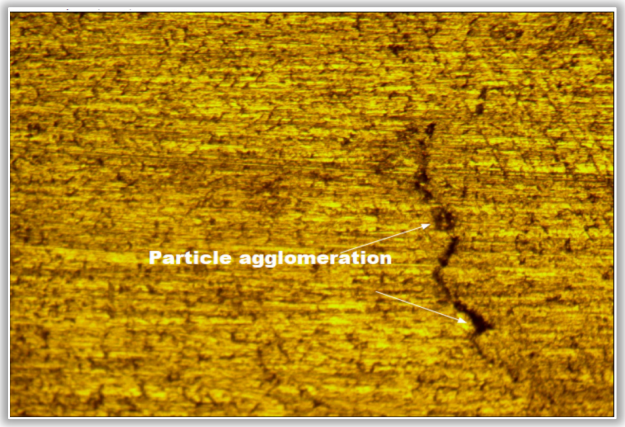

Figure 9(g). AA2011 + 2 wt. % metakaolin

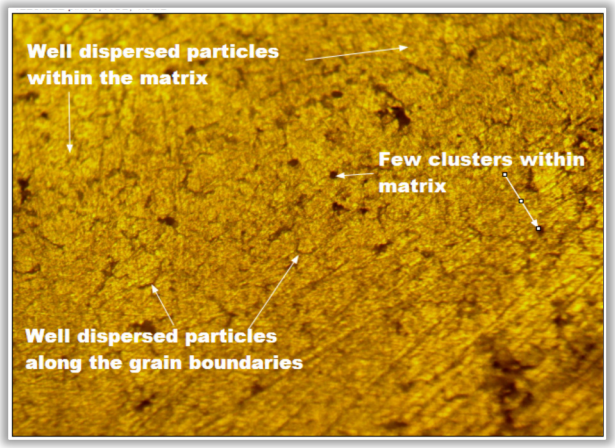

Figure 9(h). AA2011 + 4 wt. % metakaolin

Figure 9(i). AA2011 + 6 wt. % metakaolin

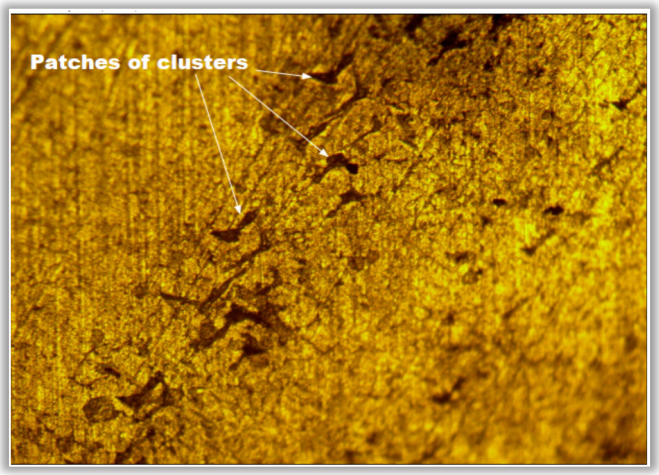

Figure 9(j). AA2011 + 8 wt. % metakaolin

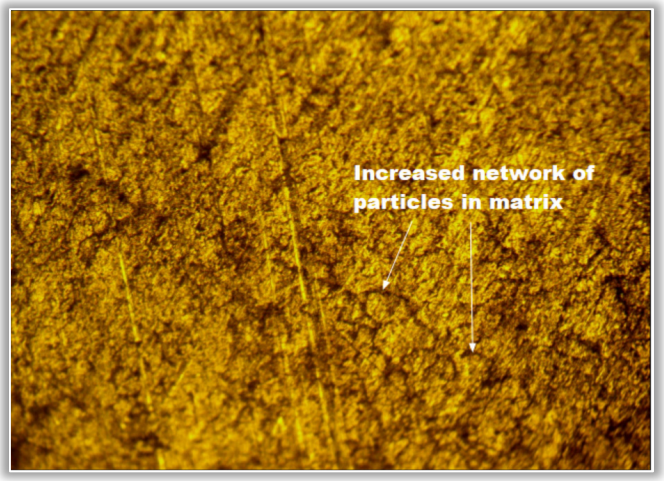

Figure 9(k). AA2011 + 10 wt. % metakaolin

Figure 9(d), shows the micrograph of AA2011 + 6 wt. % kaolin. There is agglomeration within the matrix and along the grain boundaries coupled with kaolin particles sparsely dispersed within the composite leading to microporosities within the composite. There is an increase in kaolin reinforcement in the AA2011 + 8 wt. % kaolin, which is evenly distributed along the grain boundaries as seen in Figure 9(e).

Figure 9(f) shows microporosities in the composite with AA2011 + 10 wt. % kaolin. The reinforcement is sparsely dispersed along the grain boundaries and within the matrix.

There is porosity due to the agglomeration of metakaolin particles in AA2011 + 2 wt. % metakaolin as seen within the matrix in Figure 9(g). Few reinforcements are dispersed within the matrix and along the grain boundaries.

In Figure 9(h), metakaolin particles are well dispersed within the matrix in AA2011 + 4 wt. % metakaolin and along the grain boundaries. Compared to the other composites under investigation, it has the least microporosities.

The metakaolin particles in AA2011 + 6 wt. % metakaolin is well distributed in the composite and along the boundaries as seen in Figure 9(i).

Conversely, there are patches of clusters concentrated unevenly leading to microporosities within the matrix with AA2011 + 8 wt. % metakaolin reinforcement in Figure 9(j).

There is an increased amount of metakaolin particles within the matrix and grain boundaries in the AA2011 + 10 wt. % metakaolin composite as shown in Figure 9(k). Only a few clusters can be seen within the composite matrix.

Tensile Strength Evaluation

The results obtained from the tensile tests are shown in Table 2 and Figure 10(a) – (c) respectively. Figure 10(a) looks at the tensile strength of AA2011 without reinforcement where the UTS (ultimate tensile strength) peaked at 95 MPa. The UTS dropped to 70 MPa with AA2011 + 2 wt. % kaolin. It then increased with AA2011 + 4 wt. % kaolin. The UTS dropped again to 54 MPa with 6 wt. % kaolin. With AA2011 + 8 wt. % kaolin the UTS increased again to peak at 79MPa. The lowest UTS was at AA2011 + 10 wt. % kaolin.

Figure 10(a) also shows that the least UTS with metakaolin reinforcements was at 46 MPa and 48 MPa for AA2011 + 2 wt. % metakaolin and AA2011 + 8 wt. % metakaolin respectively. The highest UTS for the metakaolin samples was with AA2011 + 4 wt. % metakaolin at 91 MPa.

There was a drop to 86 MPa with AA2011 + 6 wt. % metakaolin. The UTS of 68 MPa occurred with AA2011 + 10 wt. % metakaolin. Figure 10(b) looks at the percentage elongation of the various samples at different weight percentages of reinforcements.

Table 4. Tensile strength vs Weight % Filler

Weight % Filler	Ultimate Tensile Strength (Mpa)		% Elongation		Young Modulus (Mpa)	
	Kaolin	Metakaolin	Kaolin	Metakaolin	Kaolin	Metakaolin
0%	95.02	95.02	32.28	32.28	384.9	384.9
2%	69.76	46.24	23.39	17.81	359.88	266.1
4%	75.88	91.4	26.44	40.3	344.37	320.11
6%	54.25	85.75	19.66	29.38	281.62	377.69
8%	79.49	47.9	28.9	17.6	333.43	287
10%	45.3	67.82	17.45	23.75	273.94	329.66

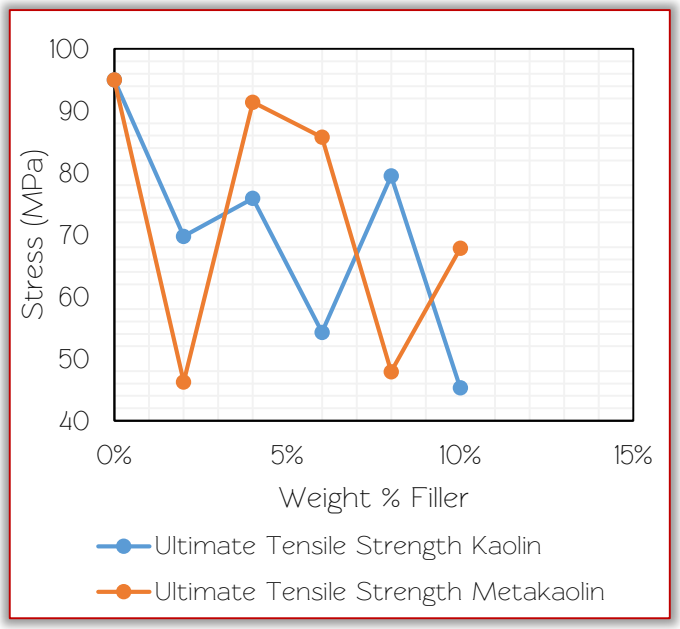

Figure 10a. Ultimate Tensile Strength vs Weight % Filler.

The percentage elongation for control AA2011 was 32.3%. There was a steady increase initially with kaolin reinforcement in AA2011 + 2 wt. % kaolin at 23.4%. This increased to 26.4% with AA2011 + 4 wt. % kaolin but declined to 19.7% with AA2011 + 6 wt. % kaolin and then spiked up to 28.9% with AA2011 + 8 wt. % kaolin. It eventually dipped to its lowest elongation at 17.5% with AA2011 + 10 wt. % kaolin.

The AA2011 + 2 wt. % metakaolin and AA2011 + 8 wt. % metakaolin showed the lowest elongation at 17.8% and 17.6% respectively.

The highest elongation occurred in AA2011 + 4 wt. % metakaolin at 40.3% while the AA2011 + 6 wt. % metakaolin had an elongation of 29.4%. The improved ductility could be as a result of the metakaolin acting as grain refiners, limiting grain growth during heat treatment [25, 26].

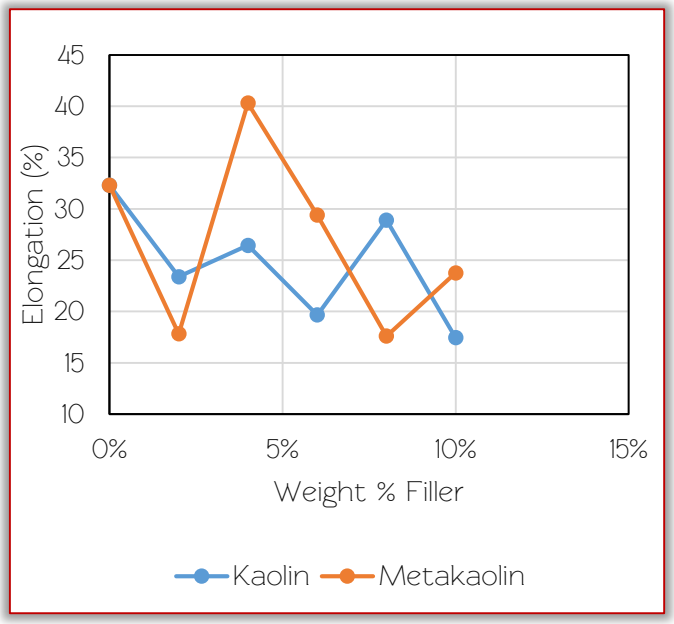

Figure 10b. Elongation vs Weight % Filler.

Results of the Young modulus of the AA2011 reinforced composites samples are depicted in Figure 10 (c). The Young modulus of the control AA2011 was 385 MPa. AA2011 + 2 wt. % kaolin had the highest value of Young modulus at 360 MPa. This value dropped to 344 MPa with AA2011 + 4 wt. % kaolin. There was a further drop to 282 MPa with AA2011 + 6 wt. % kaolin. This value increases to 333 MPa with AA2011 + 8 wt. % kaolin and then drops to its lowest of 274 MPa with AA2011 + 10 wt. % kaolin.

In AA2011 + 2 wt. % metakaolin, the Young modulus is 266 MPa. There was a steady increase from that point as shown in Figure 10 (c) where the Young modulus value for AA2011 + 4 wt. % metakaolin reinforcement was 320 MPa. There was a further increase to a peak of 378 MPa with AA2011 + 6 wt. % metakaolin. This value dropped to 287 MPa with AA2011 + 8 wt. % metakaolin before it increased to 330 MPa with AA2011 + 10 wt. % metakaolin.

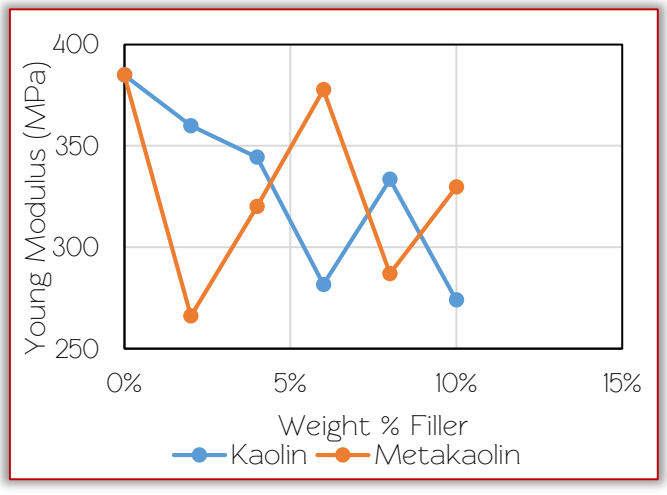

Figure 10c. Young Modulus vs Weight % Filler

Thermogravimetric Analysis (TGA)

Table 5 shows data obtained from the thermogravimetric analysis (TGA) of AA2011 with varying weight percentages of kaolin and metakaolin.

Table 5. TGA values of AA2011 with varying weight % kaolin and metakaolin reinforcement

	0% Filler	4% K	4% Me	8% Me	10% Ka
Temp range (°C)	30 – 950	30 – 660	30 – 660	30 – 660	30 – 950
Initial mass (mg)	20.93	20.39	20.70	20.39	20.52
Onset temp (°C)	200	220	200	220	560
1st Mass loss (%)	12	88	84	87	45
2nd Mass loss (%)	71	0	0	0	0
Total mass loss (%)	83	88	84	87	45
Residue (%)	17	12	16	13	55

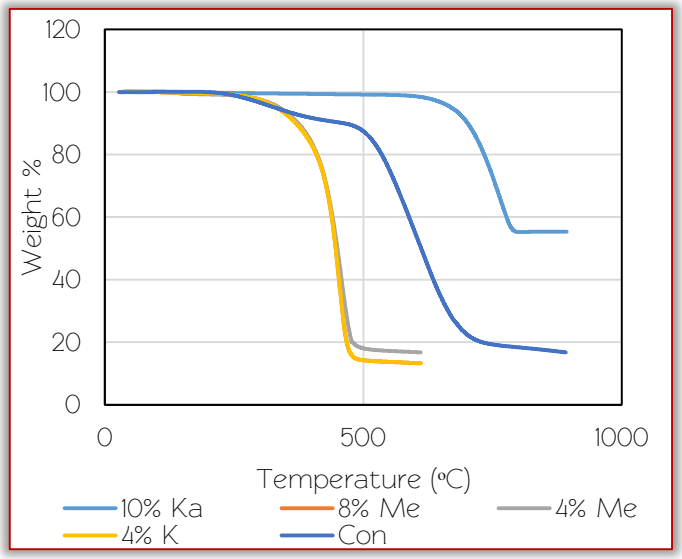

Figure 11a. TGA values of AA2011 with varying weight % kaolin and metakaolin reinforcement.

Figure 11(a) also shows the corresponding TGA curve from the analysis. It can be seen from Figure 11(a) that AA2011 without reinforcement and AA2011 + 4 wt. % metakaolin have onset temperatures of 200°C respectively. They both have a total mass loss of 83% and 84% while their residual masses are 17% and 16% respectively. Meanwhile, AA2011 + 4 weight % kaolin and AA2011 + 8 wt. % metakaolin have higher onset temperatures of 220°C with a total mass loss of 88% and 87% respectively, while their residual masses are 12% and 13% respectively. AA2011 + 10 weight % kaolin had the highest onset temperature of 550°C indicating it is more thermally stable than the other composites under investigation. This is corroborated by the lower total mass loss of 45% and a residual mass of 55%. The higher residual mass indicates the composite's formation of non–volatile compounds or more stable oxides. This is consequent on the formation of a protective thermally stable aluminium oxide layer at elevated temperatures reducing further oxidation and mass loss during TGA. This substantial residual mass could be because of higher ceramic content owing to kaolin addition [27, 28].

Figure 11(b) shows the corresponding DTG (Differential Thermogravimetric) curve from the TGA analysis. It can be seen from Figure 11(b) that AA2011 has two endothermic peaks indicating points of phase transformations [29]. The first peak, where the first transformation takes place at 300°C has the lowest percentage weight loss of 0.5%/min among others in this investigation. The second peak occurred at 600°C with a percentage weight loss of 4%/min, indicating more rapid weight change. Phase change occurred at 440°C with AA2011 + 4 wt. % kaolin percentage with a weight loss of 9%/min. At 448°C, AA2011 + 4 wt. % metakaolin undergoes a phase transformation with weight loss at 9.5%/min. There was phase transformation in AA2011 + 8 wt. % metakaolin at 442°C with weight loss at its highest rate of 11%/min. At 770°C, there was a phase transformation in AA2011 + 10 wt. % kaolin at a weight loss rate of 4.3%/min. Phase transformation occurred at this point and is higher than the 600°C of unreinforced AA2011. This suggests the thermal stability of this composite combined with its slow rate of weight loss.

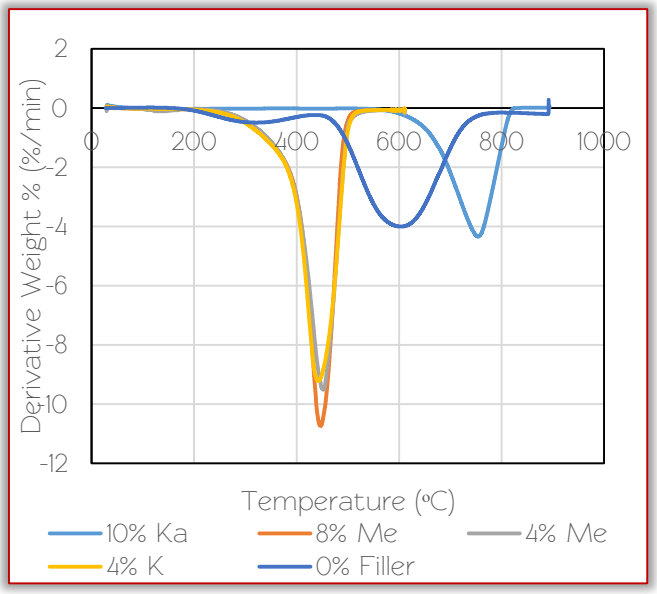

Figure 11b. DTA curve of AA2011 composites.

Electrical Conductivity

To study the effect of current on the electrical conductivities of AA2011 alloy samples reinforced with varying weight percentages of metakaolin and kaolin fillers, applied currents of 10 A, 20 A, 50 A, 100 A, 200 A, 300 A, 400 A, and 500 A were applied to the each of the samples. The results of the conductivities in kilosiemens per meter (kS/m) are shown in Table 6.

Table 6. Conductivities of AA2011 in kilosiemens per meter (kS/m) with varying weight % kaolin and metakaolin reinforcement at different applied currents.

	Conductivity of Sample (kS/m)			
Current(A)	10A	20A	50A	100A
0% Filler	80.65	74.07	69.44	67.57
4% Me	87.72	78.13	72.99	70.92
8% Me	63.29	55.25	51.55	50.25
8% Ka	81.97	71.43	66.23	64.52
10% Ka	100.00	88.50	81.30	78.74

	Conductivity of Sample (kS/m)			
Current(A)	200A	300A	400A	500A
0% Filler	66.67	65.36	64.10	62.89
4% Me	69.93	69.44	68.49	67.57
8% Me	49.50	49.02	48.54	47.85
8% Ka	63.69	62.89	62.50	62.11
10% Ka	77.52	76.34	75.19	73.53

Figure 11 shows an inverse relationship between applied currents and electrical conductivities for all the samples. This phenomenon is due to the Joules effect which is typical for all metals. In AA2011 without reinforcement, it can be observed that the electrical conductivity was dropping as the applied current was increasing. However, the electrical conductivity of AA2011 + 4 wt. % metakaolin was higher than the control at all applied currents. This shows that little addition of metakaolin increases the conductivity of AA2011. With further increase in the level of metakaolin, using AA2011 + 8 wt. % metakaolin sample, the electrical conductivity was observed to be lower than the control, and it also had the least values among all the samples at all applied currents. The reduction in electrical conductivity is expected as the filler content increases. This is due to the insulating nature of ceramics [30].

The electrical conductivity of AA2011 + 8 wt. % kaolin was slightly lower than that of the control sample at all applied currents except at the lowest current where it was higher. On the contrary, AA2011 + 10 wt. % kaolin sample had the highest electrical conductivity value among all the samples at all applied currents, peaking at 100kS/m at 10A. This result suggests optimal filler content for improving electrical performance at low currents.

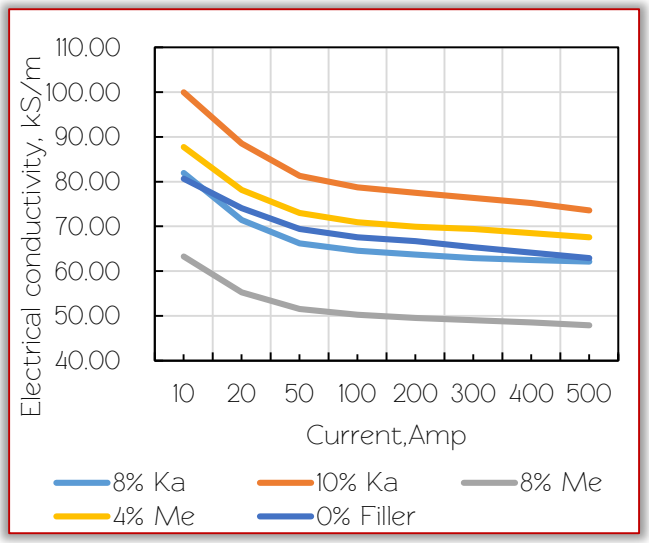

Figure 12. Electrical conductivity of AA2011 with varying weight percent of reinforcements

Statistical Analysis (Analysis of Variance)

To further ascertain the impact of kaolin and metakaolin on the mechanical properties of the AA2011 composite, variance analysis (one–way ANOVA) has been adopted. A null hypothesis H_0: Meaning there is no effect of one variable on the other and alternate hypothesis H1: at the level of significance $\alpha = 0.05$ were set up following the assumption of the Shapiro–Wilk Test [31]. The ANOVA Table # further describes the significance level of each reinforcement on the tensile strength as obtained using a statistical calculator.

Considering the effect between groups, the P–value of 0.8385 > a and F–statistics 0.04376 < F–critical 2.49 indicates that the difference between the sample averages of all groups is not big enough to be statistically significant hence, H_0 cannot be rejected. By implication, though there exists a variation in mean between groups, the difference is minimally small to be significant. This deduction complements the result predicted by the tensile experiment.

Table 7: One–way ANOVA

Source of Variation	Degrees of freedom (df)	Sums of Squares (SS)	Mean Squares (MS)	F–Statistics	F–Critical	P–Value
Groups (between groups)	1	17.3521	17.3521	0.04376	4.9700	0.8385
Error (Within groups)	10	3965.2768	396.5277			
Total	11	362.0572	362.0572			

A comparison of the impact of the two reinforcing components kaolin and metakaolin based on the statistical analysis shows that neither kaolin nor metakaolin outperformed each other as there is no significant variation in mean. Also, their effect had a downward tow on the tensile strength of the reinforced composite.

CONCLUSION

Reinforcement of the AA2011 aluminum matrix with kaolin and metakaolin was successfully carried out. Inference from the various analyses established that reinforcement of AA2011 with kaolin and metakaolin significantly decreased the ultimate tensile strength of the composite. However, at certain filler concentrations, the reduction in ultimate tensile strength was a tradeoff for ductility, and thermal and electrical conductivity as these parameters were improved following the addition of these reinforcements.

Furthermore, this experiment confirmed heat treatment as a potential tool for enhancing the ductility of AA2011 composites. Although, the addition of kaolin and metakaolin improved the thermal stability of the composite, however, the presence of kaolin in the matrix of AA2011 demonstrated a higher stability, making it suitable for applications requiring high thermal stability.

References

[1] Ye, T., Xu, Y., & Ren, J. "Effects of SiC particle size on mechanical properties of SiC particle reinforced aluminum metal matrix composite." Materials Science and Engineering: A, 753, 146–155, 2019.

[2] Verma, S., & Rao, S. "Study on mechanical behavior of aluminum alloy 6061 based composites a review." IOSR J Mechanic Civil Eng, 15(4), 16–20, 2018.

[3] Kotteda, T. K., Eshwar, D., Balakrishna, G., Kuchampudi, S. V., Prasad, B. D., & Sadasivam, S. "Experimental investigation on metal matrix nanocomposite: aluminium alloy 6061 and 7075 with SiC and Fly Ash." Journal of Nanomaterials, 2022(1), 8368934, 2022.

[4] Rajesh, S., Kumar, R. S., Madhankumar, S., Sheshan, M., Vignesh, M., & Kumar, R. S. Study of the mechanical properties of Al7075 alloy, silicon carbide and fly ash composites manufactured by stir casting technique. Materials Today: Proceedings, 45, 6438–6443, 2021.

[5] Cong, P., & Cheng, Y. "Advances in geopolymer materials: A comprehensive review." Journal of Traffic and Transportation Engineering, 8, 283–314, 2021.

[6] Jiang, X., Zhang, Y., Xiao, R., Polaczyk, P., Zhang, M., Hu, W., Bai, Y., & Huang, B. "A comparative study on geopolymers synthesized by different classes of fly ash after exposure to elevated temperatures." Journal of Cleaner Production, 270, 122500, 2020.

[7] Singla, R., Senna, M., Mishra, T., Alex, T.C., & Kumar, S. "High strength metakaolin/epoxy hybrid geopolymers: Synthesis, characterization and mechanical properties." Applied Clay Science, 221, 106459, 2022.

[8] Wang, H., Yan, C., Li, D., Zhou, F., Liu, Y., Zhou, C., & Komarneni, S. "In situ transformation of geopolymer gels to self–supporting NaX zeolite monoliths with excellent compressive strength." Microporous and Mesoporous Materials, 261, 164–169, 2018.

[9] Król, M., & Mozgawa, W. "Zeolite layer on metakaolin–based support." Microporous and Mesoporous Materials, 282, 109, 2019.

[10] Wu, Y., Luo, S., Wu, J., Guo, B., Wu, Z., Chen, B., Yu, Z., Zhang, Z. & Li, W. Development and characterization of CrCoNi medium entropy alloy particles reinforced aluminum matrix composite. Crystals, 12(10), p.1452, 2022.

[11] Soltani, S., Azari Khosroshahi, R., Taherzadeh Mousavian, R., Jiang, Z. Y., Fadavi Boostani, A., & Brabazon, D. Stir casting process for manufacture of Al–SiC composites. Rare Metals, 36, 581–590, 2017.

[12] Wang, Y., & Zhang, J. "A Review of the Friction and Wear Behavior of Particle–Reinforced Aluminum Matrix Composites." Lubricants, 11(8), 317, 2023.

[13] Sahu, M. K., & Sahu, R. K. "Fabrication of aluminum matrix composites by stir casting technique and stirring process parameters optimization." Advanced casting technologies. Intechopen, 2018.

[14] Sonsoles de Soto, I., Casas, M., & García–Giménez, R. "Evolution of Metakaolin Thermal and Chemical Activation from Natural Kaolin." Minerals, 10(6), 534, 2020.

[15] Mohammed, G., Hammajam, A., & Mshelia, Z. "Effects of modified kaolin on mechanical properties of aluminium metal matrix composite." Nigerian Journal of Engineering Science and Technology Research, Vol. 9, No. 1, 205–214, 2023.

[16] Ogunrinola, Iyanuoluwa, Akinyemi, Marvel, Aizebeokhai, Ahzegbobor, Sule, Rasidi, Sanni, Samuel, Boyo, Henry, Omeje, Maxwell and Babalola, Philip. "Silica and kaolin reinforced aluminum matrix composite for heat storage." Reviews on Advanced Materials Science, vol. 62, no. 1, pp. 20220305, 2023.

[17] Wazeer, A., Das, A., Abeykoon, C., Sinha, A., & Karmakar, A. "Composites for electric vehicles and automotive sector: A review." Green Energy and Intelligent Transportation, 2(1), 100043, 2023.

[18] Tash, M.M., & Mahmoud, E.R.I. Development of *in–Situ* Al–Si/$CuAl_2$ Metal Matrix Composites: Microstructure, Hardness, and Wear Behavior. *Materials*. 9(6):442. 2016.

[19] Massimiliano, B. & Roberto G. "Hard anodizing of AA2011–T3 Al–Cu–Pb–Bi free–cutting alloy: improvement of the process parameters" Corrosion Science,Volume 141,63–71, 2018.

[20] Villavicencio, J., Ulloa, N. Lozada, L., Moreno, M. & Lidia Castro. The role of non–metallic Al2O3 inclusions, heat treatments and microstructure on the corrosion resistance of an API 5L X42 steel, Journal of Materials Research and Technology, Volume 9, Issue 3, Pages 5894–5911, 2020,

[21] Novák, P. Vanka, T., Nová, K.,& Stoulil, J., Průša, F., Kopeček, J., Ceballos R.D. & Laufek, F, "Structure and Properties of Fe–Al–Si Alloy Prepared by Mechanical Alloying." Materials. 12. 2463. 2019.

[22] Gonfa, B.K., Sinha, D., Vates, U.K., Badruddin, I.A., Hussien, M., Kamangar, S., Singh, G.K., Ahmed, G.M.S., Kanu, N.J., and Hossain, N. "Investigation of Mechanical and Tribological Behaviors of Aluminum Based Hybrid Metal Matrix Composite and Multi–Objective Optimization." Materials, 15(16):5607, 2022.

[23] Cao, H., Luo, Z., Wang, C., Wang, J., Hu. T, Xiao, L. & Che, J. "The Stress Concentration Mechanism of Pores Affecting the Tensile Properties in Vacuum Die Casting Metals." Materials (Basel). 6(13):3019, 2020.

[24] Rajkumar, K., & Aravindan, S. "Tribological performance of microwave sintered copper–TiC–graphite hybrid composites." Tribology International, 44(4), 347–358, 2011.

[25] Adeosun, S.O., Oyetunji, A., & Akpan, E.I. "Strength and ductility of forged 1200 aluminum alloy reinforced with steel particles." Nigerian Journal of Technology, 34(4), 710–715, 2015.

[26] Adeosun, S. O., Balogun, S.A., Sanni O. S., & Ayoola, W.A. "Improving the Strength and Ductility of Wrought Aluminum through Particle addition." Proceedings of Materials Science and Technology (MS&T), October 25–29, 1918 – 1928, 2009.

[27] Owais A. W., & Ho J. R., "Combinatorial synthesis and analysis of AlxTayVz–Cr20Mo20Nb20Ti20Zr10 and Al10CrMoxNbTiZr10 refractory high–entropy alloys: Oxidation behavior." Journal of Alloys and Compounds, Volume 828, 154427, 2020

[28] Butler, T.M., Chaput, K.J., Dietrich J.R., Senkov, O.N. "High temperature oxidation behaviors of equimolar NbTiZrV and NbTiZrCr refractory complex concentrated alloys (RCCAs)," Journal of Alloys and Compounds. 729, 1004–1019, 2017.

[29] Neeraj, D., Shobhit, S., Bhumika, Y., & Sujeet K.G. "A Review on Differential ThermalAnalysis", 2021.

[30] Khan, I., & Khalil, F.H. "Influence of SiC particles on the physical properties of Al–SiC composites." Journal of Materials Processing Technology."166(3). 273 – 278, 2005.

[31] Mishra P.; Pandey C., Singh U., Gupta A., Sahu C. & Keshri A. "Descriptive statistics and normality tests for statistical data". Ann Card Anaesth." 22(1). 67–72. 2019.

ISSN: 2067–3809